BJR

https://doi.org/10.1259/bjr.20230189

Received: 21 February 2023 | Revised: 29 August 2023 | Accepted: 30 August 2023 | Published online: 25 October 2023

Cite this article as:
Horst KK, Yu L, McCollough CH, Esquivel A, Thorne JE, Rajiah PS, et al. Potential benefits of photon counting detector computed tomography in pediatric imaging. *Br J Radiol* (2023) 10.1259/bjr.20230189.

REVIEW ARTICLE

Potential benefits of photon counting detector computed tomography in pediatric imaging

[1]KELLY K. HORST, MD, [2]LIFENG YU, PhD, [2]CYNTHIA H. MCCOLLOUGH, PhD, [2]ANDREA ESQUIVEL, MD, [2]JAMISON E. THORNE, [2]PRABHAKAR SHANTA RAJIAH, MBBS, MD, [2]FRANCIS BAFFOUR, MD, [1]NATHAN C. HULL, MD, [2]NIKKOLE M. WEBER, RT(R)(CT), [1]PAUL G. THACKER, MD, MHA, [1]KRISTEN B. THOMAS, MD, [1]LARRY A. BINKOVITZ, MD, [2]JULIE B. GUERIN, MD and [2]JOEL G. FLETCHER, MD

[1]Pediatric Radiology Division, Department of Radiology, Mayo Clinic, Rochester, United States
[2]Department of Radiology, Mayo Clinic, Rochester, United States

Address correspondence to: Dr Kelly K. Horst
E-mail: *horst.kelly@mayo.edu*

ABSTRACT

Photon counting detector (PCD) CT represents the newest advance in CT technology, with improved radiation dose efficiency, increased spatial resolution, inherent spectral imaging capabilities, and the ability to eliminate electronic noise. Its design fundamentally differs from conventional energy integrating detector CT because photons are directly converted to electrical signal in a single step. Rather than converting X-rays to visible light and having an output signal that is a summation of energies, PCD directly counts each photon and records its individual energy information. The current commercially available PCD-CT utilizes a dual-source CT geometry, which allows 66 ms cardiac temporal resolution and high-pitch (up to 3.2) scanning. This can greatly benefit pediatric patients by facilitating high quality fast scanning to allow sedation-free imaging. The energy-resolving nature of the utilized PCDs allows "always-on" dual-energy imaging capabilities, such as the creation of virtual monoenergetic, virtual non-contrast, virtual non-calcium, and other material-specific images. These features may be combined with high-resolution imaging, made possible by the decreased size of individual detector elements and the absence of interelement septa. This work reviews the foundational concepts associated with PCD-CT and presents examples to highlight the benefits of PCD-CT in the pediatric population.

INTRODUCTION

Since its introduction into medicine over 50 years ago, the technology used in CT scanners has undergone many dramatic changes, enabling single breath-hold scanning of the body, stop-motion imaging of the heart, and quantitative imaging using dual-energy techniques. Energy-resolving, photon-counting detector (PCD) CT is the latest advance in CT technology. It differs from all earlier CT systems, which used energy integrating detectors (EIDs), in the way that X-rays are converted to electronic signals. Among the advantages of PCD-CT is increased dose efficiency, which permits a reduction in radiation dose relative to EID-CT while maintaining or improving image quality.[1–5] Additional benefits include improvements in spatial resolution, increased iodine signal, and reduced electronic noise.[6–16]

The first PCD-CT system to become commercially available (NAEOTOM Alpha, Siemens Healthineers, Forchheim, Germany) utilizes a dual-source geometry.[7] Because children are generally more prone to movement during scan acquisition than are adult patients, pediatric CT protocols tend to prioritize rapid image acquisition to reduce motion artifacts, in addition to radiation dose reduction.[17–21] Dual-source CT offers one method to optimize scan speed, where two X-ray tube/detector pairs scan overlapping body regions at high table speeds, achieving a temporal resolution that is a factor of two superior to single-source geometries.[22] These dual-source, high-pitch (up to 3.2) "Flash" scans have the potential for subsecond scans times (depending on body region) and per image temporal resolution as fast as 66 ms.[23] While these speeds match current dual-source EID-CT capabilities, the use of PCDs allows for simultaneous multienergy imaging, providing the ability to perform multienergy imaging with high-pitch, high-temporal resolution or ultra-high spatial resolution.[7,24–27] Table 1 offers sample protocols for pediatric patients that demonstrate these advantages. This combination of capabilities optimizes CT image quality in

Table 1. Sample protocols

	CARE Dose4D & CARE keV	CARE keV optimized for	CARE keV IQ level	Effective mAs	kV	Pitch	Rotation time (s)	Scan modea (short name)	Collimation (mm)	Kernel
Chest without contrast	Manual	Non-contrast	35–45	Varies	120	3.2	0.25	Flash+SR+ME or Flash+UHR	144 × 0.4 (SR) or 120 × 0.2 (UHR)	Br44, Qr56
Chest with contrast	Manual	Soft Tissue	35–45	Varies	120	3.2	0.25	Flash+SR+ME	144 × 0.4	Br44, Qr56
Chest without contrast (low dose)	Manual	Non-contrast	2–6	Varies	100Sn	3.2	0.25	Flash+UHR+Sn	120 × 0.2	Br44, Qr56
Abdomen Pelvis with contrast	Manual	Soft Tissue	120–140	Varies	120	3.2	0.25	Flash+SR+ME	144 × 0.4	Br44, Qr44
Abdomen Pelvis without contrast	Manual	Non-contrast	120–140	Varies	120	3.2	0.25	Flash+SR+ME	144 × 0.4	Br44
Extremity without contrast	Off	Off	Off	65–160	120	1	0.5–1	UHR+ME	120 × 0.2	Br76 to Br84
Extremity CTA	Manual	Vascular	120–140	Varies	120	0.5	0.25–1	UHR+ME	120 × 0.2	Bv38 to Bv60
Temporal Bone without contrast	Manual	Non-Contrast	220	Varies	120	0.5	1	UHR+ME	120 × 0.2	Hr44, Hr84
Abdominal CTA	Manual	Vascular	120–180	Varies	120	0.5	0.25	UHR+ME	120 × 0.2	Bv38 to Bv60

[a]SR, standard resolution; ME, multienergy-energy; UHR, ultra-high resolution

Figure 1. (a) Schematic of an EID. EID-CT uses a scintillator to produce visible light when an X-ray photon strikes it; this light is then converted to electrical signal by a photodiode. Reflective septa are positioned between detector elements to minimize the spread of light to adjacent detector elements. (b) Schematic of a PCD. PCD-CT directly generates charge pairs (electrons and holes) using a semi-conductor, with the charges traveling across a potential difference to induce an electrical signal at the pixelated anodes. (c) A low-energy threshold (*e.g.* 20 keV) is utilized to eliminate electronic noise, which lies below that energy. A high-energy threshold (*e.g.* 65 keV) can also be set to divide the detected photons into low- and high energy data sets. EID, energy integrating detector; PCD, photon counting detector.

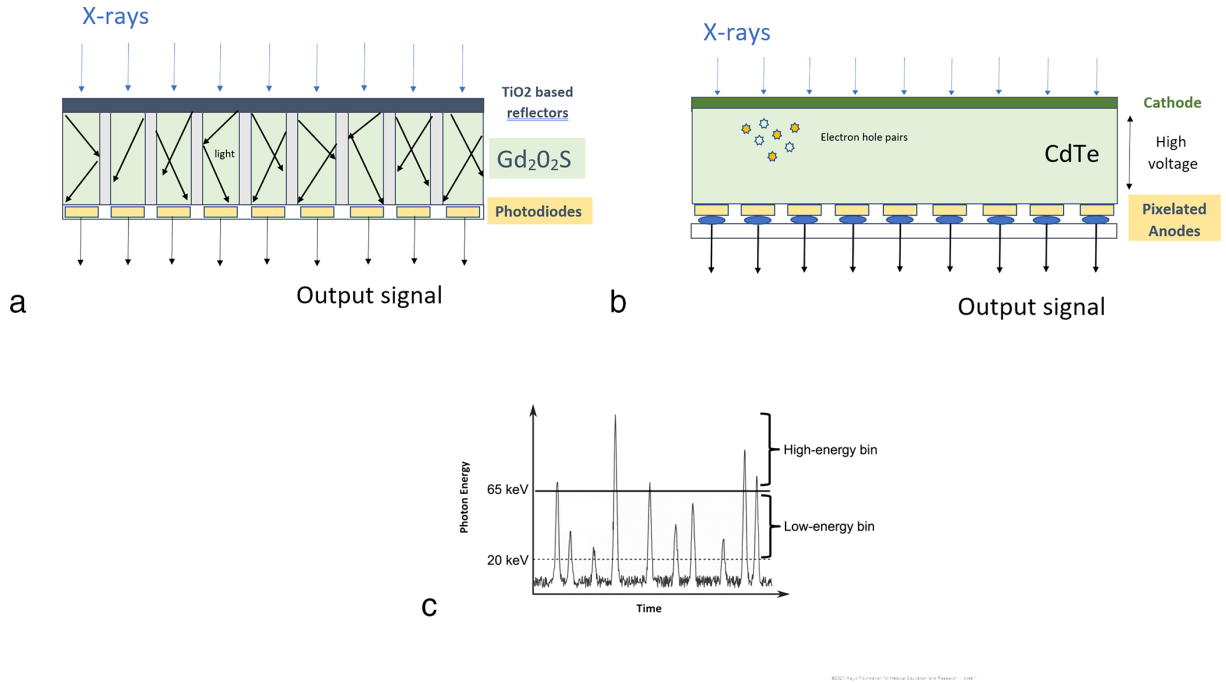

a manner that is beneficial for pediatric patients by combining simultaneous rapid imaging acquisition, multienergy capabilities, and improved spatial resolution for imaging small anatomic parts.[28–30]

This article will describe PCD-CT, detail the differences between PCD-CT and EID-CT, and illustrate current and possible future clinical applications in children.

UNIQUE FEATURES AND BENEFITS OF PHOTON-COUNTING CT DETECTORS

EID-CT uses solid-state scintillators made of materials such as gadolinium-oxysulfide, which convert X-ray photons to visible light, which is subsequently converted to electrical signal by a photodiode (Figure 1a).[7,9–11,25,31,32] The detector elements (detector pixels) are separated by reflective septa to reduce the spread of visible light to adjacent detector elements. The output signal of each detector element is the summation of the energies of all detected photons, where higher-energy photons are weighted more heavily in the total output signal.[9,10] Lower energy X-ray photons contain more inherent contrast information because they interact more frequently by the photoelectric effect, which enhances contrast in biological tissues. Low-energy photons above 33 keV are also closer to the k-edge of iodine, a point at which iodine signal strongly increases. However, in EID-CT, lower-energy photons represent a lower percentage of the total output signal from the detector, lowering the contrast-to-noise ratio (CNR) of soft tissues, bone, and iodine.[9,10]

PCD-CT utilizes semi-conductors such as cadmium zinc telluride (CZT), cadmium telluride (CdTe), or silicon (Si),[32] which enable the direct conversion of X-rays to electrical signal, without the conversion to visible light.[9–11] The theoretical feasibility of pediatric applications for photon-counting CT were first demonstrated using a Monte Carlo model with silicon detectors by Yveborg et al in 2009.[33] The current commercially available scanner (NAEOTOM Alpha; Siemens Healthineers) utilizes CdTe.[7,9,32] When an incident X-ray photon interacts with the semi-conductor material, it creates a cloud of electrons and holes, which then move across a high voltage potential to create 10–20 ns electrical pulses at the pixelated anodes (Figure 1b).[9–11,34,35] These pixelated anodes form the individual detector elements. The anodes are bonded to an application-specific integrated circuit (ASIC) that provides parallel read-out channels on the back side of the detector.[9] At higher incident photon energies, more electrons and holes are created and the signal amplitude is increased. A pulse height analyzer subsequently compares the pulse height against preset thresholds to determine which counter should be incremented (Figure 1c).[10] In this manner, the energies of different photons are resolved, rather than summed.

SYSTEM DEVELOPMENT

The development of PCD-CT has occurred over the time span of nearly 20 years and has included the creation of various small animal and human research systems. The primary technical challenge has been to fabricate in a robust and affordable manner detectors capable of operating at CT photon flux levels (up to 10^9

photons/s/mm^2). Investigational PCD-CT systems developed over the past decade include two whole-body research systems (SOMATOM Count and SOMATOM Count Plus, Siemens Healthineers), both using CdTe detectors. In two other research systems, a CZT-based detector is used (Philips Healthcare, Haifa, Israel)[36–38] and a Si-based detector is used (GE Healthcare, Chicago, IL).[39]

In 2021, a clinical high-flux-capable PCD-CT system (NAETOM Alpha) became commercially available.[7,25] It offers a range of tube potentials (70, 90, 120, 140 kV) and tube currents between 10 and 1300 mA.[25] Tin filtration is available at 100 and 140 kV. Two detector collimations are available: the standard 140 × 0.4 mm (5.76 cm coverage per rotation) and the ultra-high resolution 120 × 0.2 mm (2.4 cm coverage). Several recent publications detail the specific scan protocols used in pediatric patients.[4,28–30]

Spatial resolution improvement

The design of PCDs is such that reflective septa are not required, as they are in EIDs. This improves the geometrical dose efficiency because septa can fill about 20–30% of an EID's surface area, absorbing photons that have passed through the patient without contributing to image signal.[10]

To improve the spatial resolution of a CT system, the detector elements must become smaller. In EID-CT, this would further increase the "dead space" occupied by septa as a percentage of the detector's surface area. To achieve better resolution without taking this step, which would impose a dose penalty across all scan types, some scanners have the option of moving an ultra-high resolution attenuating grid or comb "filter" in front of the detector to decrease the effective size of the detector element by blocking incident X-rays.[40] This imposes a radiation dose penalty of approximately a factor of 2, and hence is used in only limited applications, such as imaging of the inner ear or the extremities. Given the emphasis on radiation dose reduction in pediatric CT protocols,[17,18,41] it is important to note that the detector design of PCD-CT eliminates the need for grid or comb filters.[6,8,16]

In the currently available PCD-CT, ultra-high spatial resolution can be achieved solely with the use of very small detector elements (0.151 mm by 0.176 mm), without the need for additional attenuating grids or combs, allowing creation of slice thicknesses as narrow as 0.2 mm without incurring a dose penalty.[7,9,11] Ultra-high spatial resolution imaging of the torso, such as for shoulders and pelvis imaging is therefore possible with this system.[16,42]

The spatial resolution of a CT system is measured by the modulation transfer function (MTF), which describes the ability of the system to accurately convey information as a function of spatial frequency (in line pair per cm). The current commercial PCD-CT has a 10% MTF value of 36.1 lp/cm, compared to 19.6 lp/cm on a high-resolution (0.25 mm detector element) EID system.[7,43] The limiting spatial resolution (0% value of the MTF) of the NAETOM Alpha is reported to be 40 lp/cm, which can resolve high contrast objects of approximately 0.125 mm.[7]

Figure 2. A 13-year-old male with right elbow pain underwent clinical CT. Both initial EID-CT (a) and follow-up PCD-CT (b) 6 months later show an osteochondral lesion of the capitellum. The follow-up PCD-CT shows healing changes of the OCD (arrow). The lesion is more sharply demarcated on the PCD-CT, which is routinely obtained at thinner slices and sharper kernels (0.6 mm, Br89u) than EID-CT (1 mm, Ur77u). Despite improved spatial resolution, the PCD images have similar noise and lower dose with similar scanning parameters (PCD: 36 HU, CTDIvol 6.82 mGy *vs* EID 30 HU, CTDIvol 9.16 mGy) due to smaller detector subpixels and improved dose efficiency. EID, energy integrated detector; HU, Hounsfield unit; PCD, photon counting detector.

Literature highlighting the use of PCD-CT's increased spatial resolution in pediatric applications is limited. An early study used a prototype Si-based PCD-CT to evaluate low- and high-contrast tasks on pediatric phantoms demonstrated a higher detectability index for PCD-CT over EID-CT across a range of tube potential and tube current settings.[44] The improved detectability index accounts for both the increased spatial frequency and signal-to-noise properties of PCD-CT over EID-CT.

However, there is robust evidence in the adult literature of the superior spatial resolution achieved by PCD-CT compared to EID-CT. This was shown first on phantom studies using prototype PCD systems.[8,11,36,45,46] The first musculoskeletal applications performed in animals and human cadavers showed improved visualization of bone microarchitecture on PCD-CT compared to EID-CT, including cortical and trabecular detail and nutrient canals, with substantial reductions in radiation dose and image noise.[1–3] These advantages were validated in adult patients in studies performed on the wrist, shoulder, and pelvis.[16,42] PCD-CT has improved the visualization of metastatic bony lesions from breast cancer and multiple myeloma compared to EID-CT.[47,48] Similar results are expected to be applicable to pediatric oncology as well. Figure 2 illustrates the improved spatial resolution of bony detail on images of the elbow in a pediatric patient. Figure 3 shows a scaphoid fracture that was occult on plain radiographs, but readily visible on PCD-CT.

The spatial resolution advantages of PCD-CT in musculoskeletal imaging are also applicable to temporal bone imaging. Cadaveric and adult studies have documented superior spatial resolution

Figure 3. A 10-year-old female with a history of falling on the right outstretched hand. No fractures were detected on initial radiographs (not pictured), or follow-up obtained 3 weeks after injury (a), but an MRI was recommended to exclude an occult fracture. MRI was performed a month after the injury showing a faint linear T1 hypointense (b), T2 hyperintense (c) line compatible with a nondisplaced fracture of the scaphoid despite some motion artifact. Subsequently, 3 months after injury, the patient had persistent pain and a PCD-CT scan was acquired showing a subtle longitudinal subcortical, non-displaced fracture extending through the lateral cortex (arrow) of the mid-right scaphoid shown on the coronal (d) and (e) image. PCD, photon counting detector.

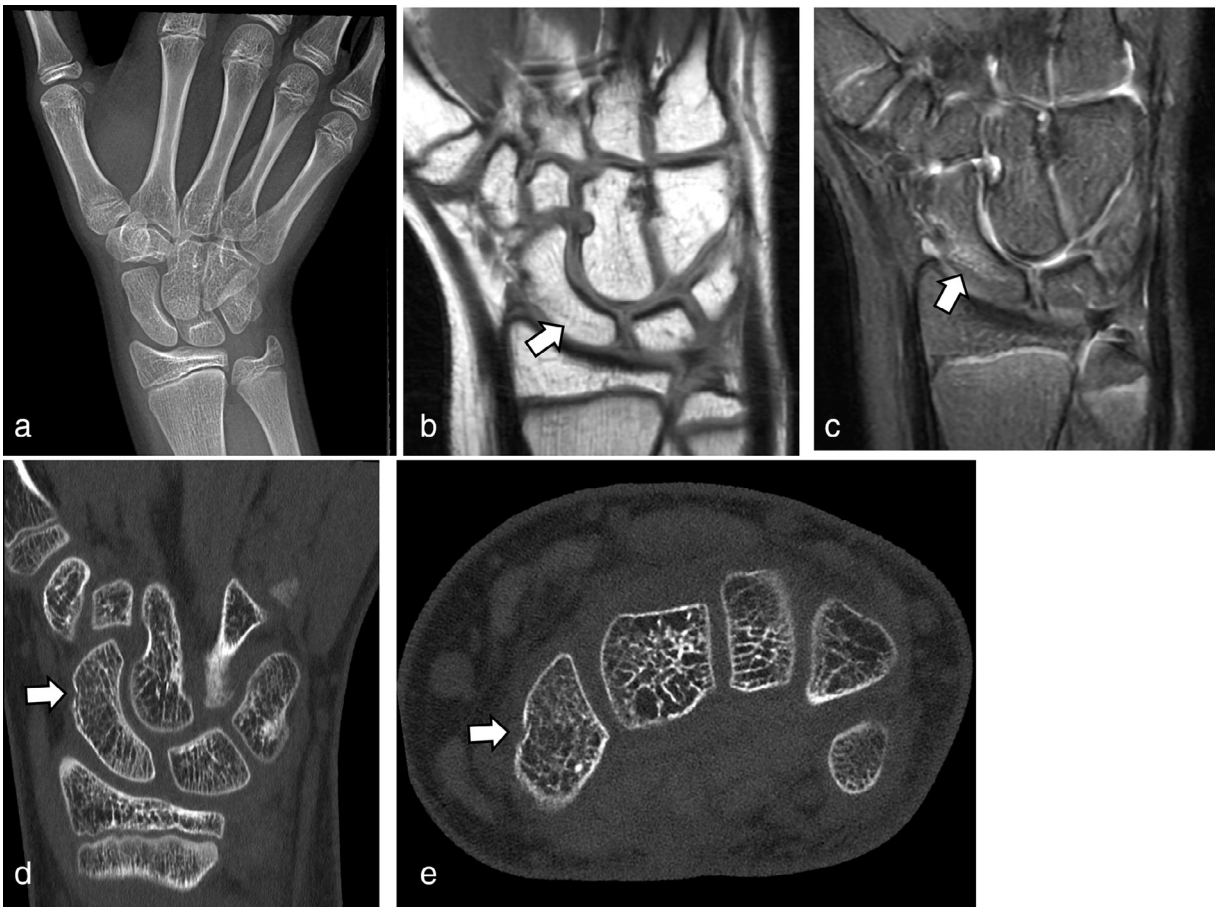

Figure 4. A 16-year-old male with a history of right cholesteatoma was imaged with PCD-CT to evaluate a right ossicular prosthesis. Images from 3D reconstruction, 0.2 mm, kernel Hr84u. The prosthesis articulates with the native stapes (arrow) which is well situated at the oval window (a). However, there is no apparent articulation laterally with the remaining ossicular chain suggesting displacement/dislocation (arrow) in (b). 3D, three-dimensional; PCD, photon counting detector.

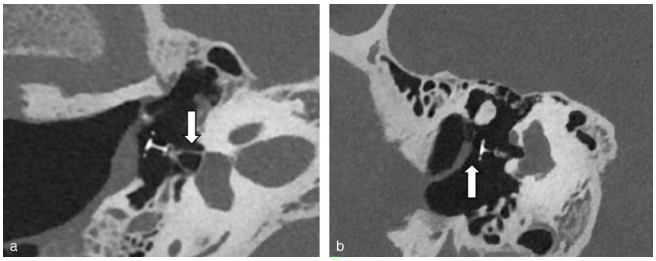

and improved ability to display the ossicular chain and incudomalleolar and incudostapedial joints at substantially lower image noise, and reduced radiation dose, through the elimination of the comb or grid attenuating filter (Figure 4).[6,49]

The increased spatial resolution of PCD-CT has also been emphasized in high-resolution imaging of the lung, where it has improved visualization of third- and fourth-order bronchi, lung nodules, and increased reader confidence in identifying reticulation, ground-glass opacities, and mosaic pattern in usual interstitial pneumonia,[50,51] with better lung nodule characterization and volume estimation.[52] Figure 5 highlights the increased spatial resolution of PCD compared to EID-CT to identify small peripheral structures in the lung of a pediatric patient with hereditary hemorrhagic telangiectasia syndrome.

Published pediatric PCD-CT studies of the lung have thus far emphasized radiation dose reduction over maximizing spatial

Figure 5. An example of multienergy chest CT with intravenous contrast acquired using the ultra-high resolution mode with a PCD-CT in a 12-year-old female with hereditary hemorrhagic telangiectasia. A previous EID-CT 0.75 mm image (a) displays only one of three small, peripheral arteriovenous malformations (arrowheads) shown on the PCD-CT 0.8 mm image (b) at the same level. In addition to high-resolution images, simultaneous multienergy acquisition on PCD-CT displays the heterogeneous perfusion of the lung parenchyma (c) and permits calculation of lung blood perfusion volume. EID, energy integrated detector; PCD, photon counting detector.

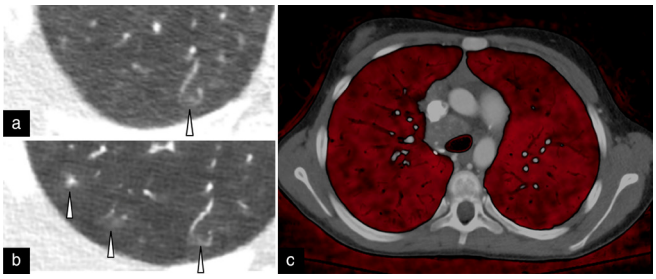

resolution.[4,29,30] Cao et al have suggested that the increased spatial resolution of PCD-CT may translate to earlier detection of metastatic lung nodules, and the added benefit of increased contrast resolution may be used to better visualize small cardiac structures in pediatric patients.[28]

RADIATION DOSE REDUCTION AND ULTRA-LOW-DOSE CT

The rapid rise of CT utilization among children in the past decades has prompted concerns regarding the potential long-term effects of ionizing radiation in this patient population.[53] Professional organizations and activities, such as Image Gently and Step Lightly, have helped to educate pediatric imaging providers on the importance of and methods for optimizing radiation doses in children,[54,55] resulting in a reduction in CT utilization in pediatric patients in the last decade.[56,57] Meanwhile, doses from CT exams continue to decrease,[58] in part due to use of newer dose reduction technologies and requirements to review CT protocols and compare doses against peer organizations.[59]

The optimization of pediatric CT protocols emphasizes radiation dose reduction and rapid scanning.[17,18,41] Multiple studies have shown a range of achievable radiation dose reductions in PCD-CT over EID-CT; the amount of reduction depending on the acquisition protocol and diagnostic task. Using a PCD prototype system to scan pediatric phantoms, Chen et al was able to show the equivalent of a 30% dose reduction for a soft tissue detection task and a 70% dose reduction for an iodine detection task.[44] In a retrospective review of 27 children who underwent PCD-CT and were compared to an age-matched cohort with the same water-equivalent diameter scanned on EID-CT, Siegel et al showed a lower median volume CT dose index (CTDIvol) of 0.41 *vs* 0.71 mGy, $p < .001$, and a lower size-specific dose estimate (SSDE) of 0.82 *vs* 1.34 mGy, $p < .001$[4], on PCD-CT compared to EID-CT. Lung attenuation, noise, and signal-to-noise ratio

Figure 6. A 6-year-old female with a history of cystic fibrosis underwent clinically-indicated PCD-CT as part of routine clinical follow-up. Coronal inspiratory (a) and expiratory (b) PCD-CT images show cylindrical bronchiectasis and air trapping, respectively in the right lower lobe. A cropped image highlights the bronchiectasis in the right lower lobe before (c) and after (d) post-processing with convolutional-neural network denoising. Scan parameters: 100 kV with a tin filter, CTDIvol: 0.05 mGy inspiration and 0.05 mGy expiration. Similarly, a 17-year-old with dyspnea and exercise-induced asthma underwent same day EID- and PCD-CT as part of a research study. (e) The dose of each inspiratory and expiratory PCD scan (CTDIvol 0.21 mGy, effective dose 0.16 mSv) is about half the dose of each EID scan shown in (f) (CTDIvol 0.43 mGy, effective dose 0.37 mSv). The air-trapping (black arrow) in the left lower lobe is well-demarcated and the mild peribronchial thickening (white arrow) in the central portions of the left upper lobe bronchi are well seen on both scan types. Similar levels of iterative reconstruction were used, with the PCD image showing less noise (PCD-CT 56 HU *vs* EID-CT 88 HU, with the ROI measured in the ascending aorta). EID, energy-integrated detector; PCD, photon counting detector.

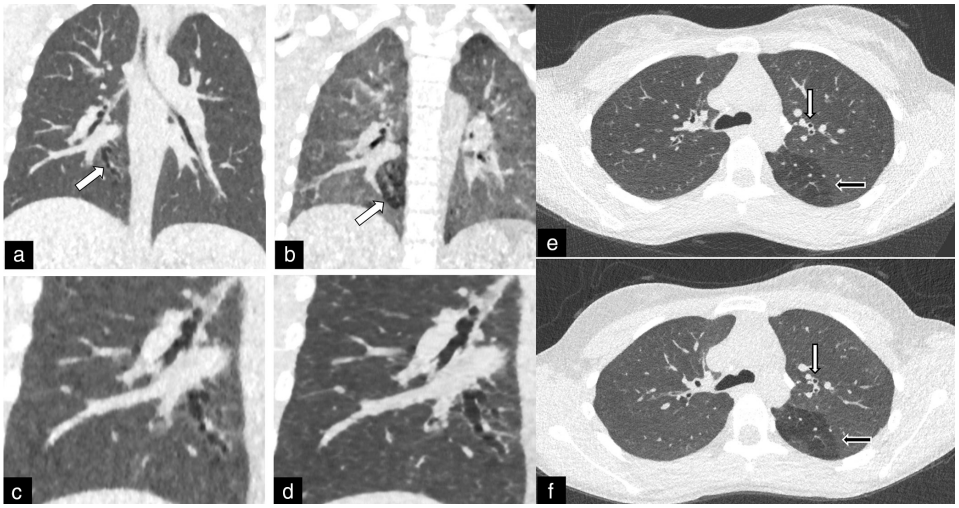

Figure 7. 10-year-old male patient with Crohn's disease. (a) Previous EID-CT scan. (b–e) PCD- CT scan. Coronal MIP images (a, b) at 8 mm show the portal vein, the PCD-CT (b) provides better visualization of the mesenteric veins as well. (c) A coronal image outlines mural hyper-enhancement and wall thickening in the J-Pouch compatible with pouchitis (arrows). A 50 keV axial image(d) illustrates how lower-energy VMIs may further optimize contrast enhancement compared to 120 kV images (e). EID-CT and PCD-CT scan parameters: 120 kV, MIP coronal images at 8 mm (a, b), coronal and axial at 2 mm slice thickness (c-e). CTDIvol 2.6 mGy (EID-CT) *vs* 1.67mGy (PCD-CT). EID, energy-integrated detector; MIP, maximum intensity projection; PCD, photon counting detector; VMI, virtual monoenergetic image.

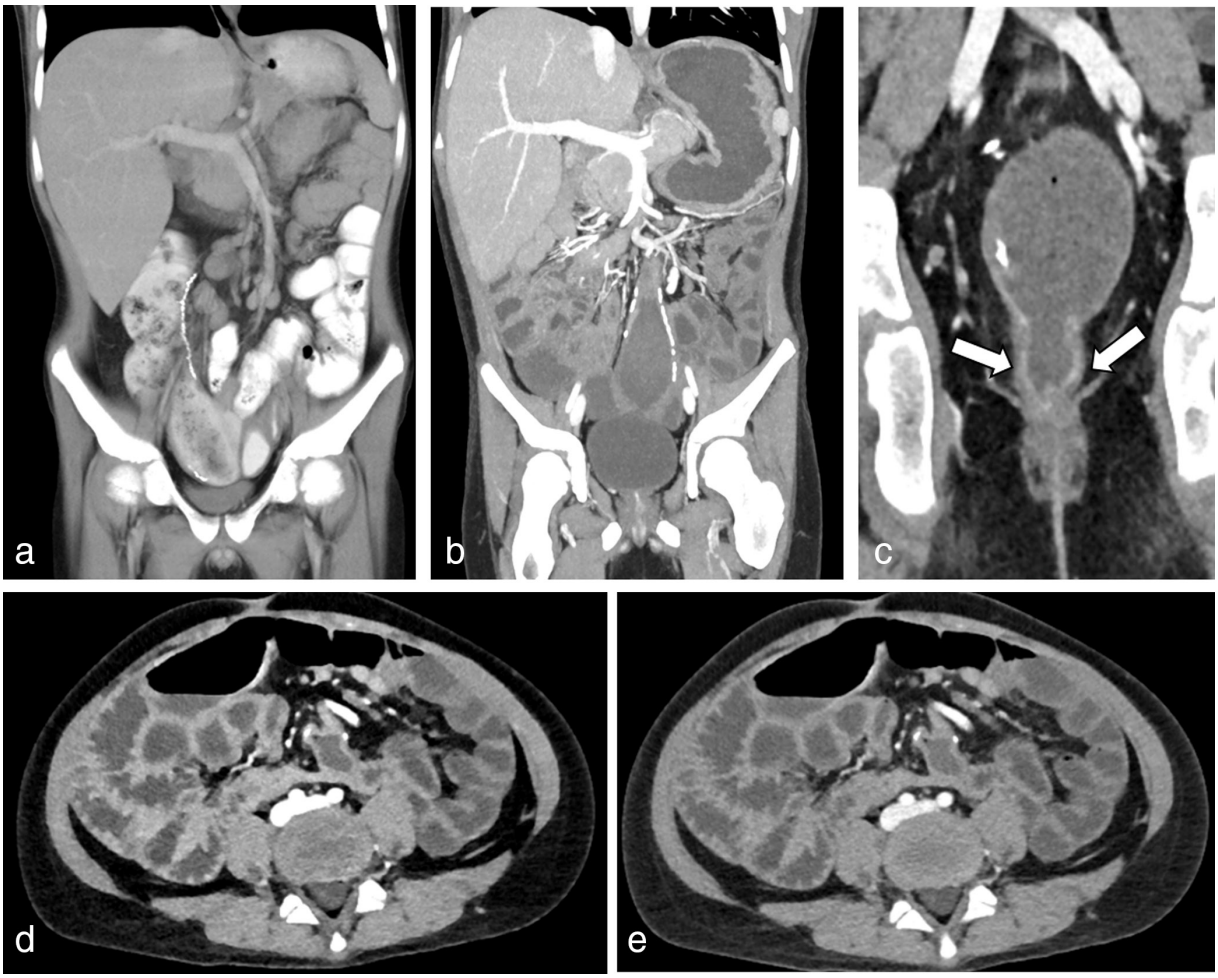

(SNR), however, were equivalent, and subjective assessment showed no differences in image quality.[4] In a study comparing contrast-enhanced chest PCD-CT performed at 90 kV to dual-source EID-CT at 70 kV in children under 3 years with congenital heart disease, PCD-CT showed equivalent radiation dose to the EID-CT scans, while increasing the SNR and CNR.[60] Likewise, numerous adult studies have shown that radiation dose may be significantly reduced in PCD-CT with similar or better image quality than EID-CT. Examples include up to a 32% dose reduction in contrast-enhanced abdominopelvic CT for general oncologic imaging,[5] a 49% dose reduction for routine CT imaging of the wrist,[16] and a 54% radiation dose reduction for the detection of focal liver lesions.[61] The dose reduction in PCD-CT is partially attributable to the elimination of septa from the detector design. Further, with an inherently higher system spatial resolution, reconstruction kernels can incorporate smoothing—which lowers noise—and still achieve the same spatial resolution as an EID-CT protocol at a lower dose. This effect is due to the small detector element size.[8,14,62–64]

A unique quality of PCD-CT that allows radiation dose reduction is its ability to eliminate electronic noise. Quantum noise arises from the stochastic (random) nature of the photon interaction processes, whereas electronic noise arises from the analog electronic circuits within the CT hardware itself.[11] In PCD-CT, a low energy threshold less than 20 or 25 keV can be set to eliminate small signals attributable to electronic noise, resulting in noticeably higher quality images at low signal levels to the detector, which occurs at low radiation doses (Figure 3).[65,66] Reduced electronic noise is also beneficial in obese patients, or in regions of the body prone to streak artifacts (*e.g.* the shoulders or pelvis), where attenuation is high. It is particularly beneficial in low-dose imaging, such as screening exams, where there is low incident photon flux and the electronic noise represents a greater proportion of the total signal.[9,11,67]

Figure 8. A 16-year-old was diagnosed with a high-grade chondroblastic osteosarcoma. A PCD- CT angiogram was performed and (a) shows severe stenosis of the proximal third of the left subclavian artery by the tumor. Using the VNC in (b), the osseous component of the tumor is identified as separate from the iodine-filled neovessels in the tumor in (a). An example of a VNCA reconstruction is shown in (c). This example showcases PCD-CT multienergy capabilities. EID, energy integrated detector; PCD, photon counting detector; VNC, virtual non-contrast; VNCA, virtual non-calcium.

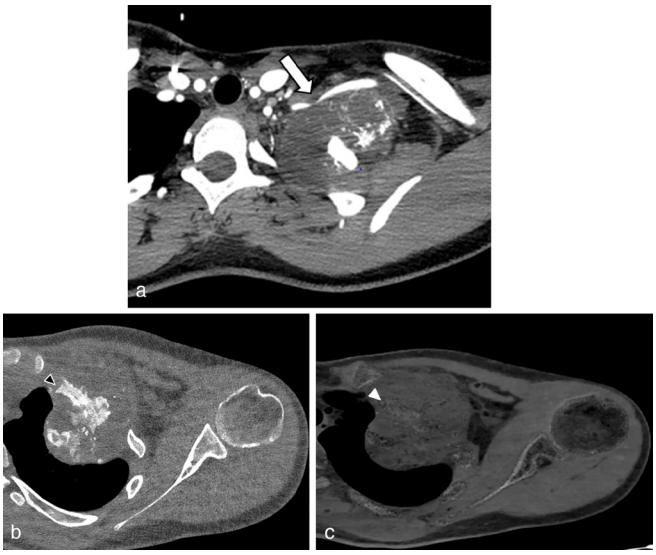

Figure 9. A 7-year-old female, also with scaphoid fracture not visible on radiograph. An axial (a) PCD-CT image of the left wrist shows cortical disruption. Virtual non-calcium images (b) were reconstructed using a proprietary algorithm that reveal increased attenuation consistent with edema/hemorrhage at the fracture site (arrow). PCD, photon counting detector.

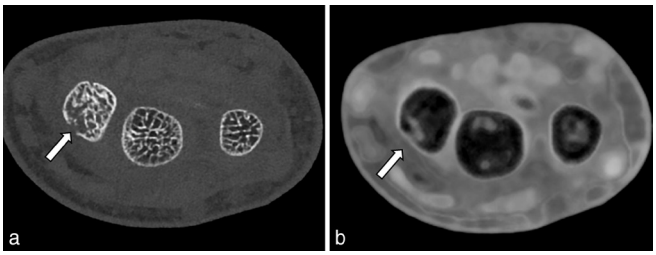

Figure 10. A 16-year-old female patient was evaluated with non-contrast CT for renal stones. There is a left staghorn calculus (a). A proprietary algorithm was used to characterize the staghorn calculus as composed of calcium oxylate (b), similar to the calcium depicted in the adjacent bony vertebral elements.

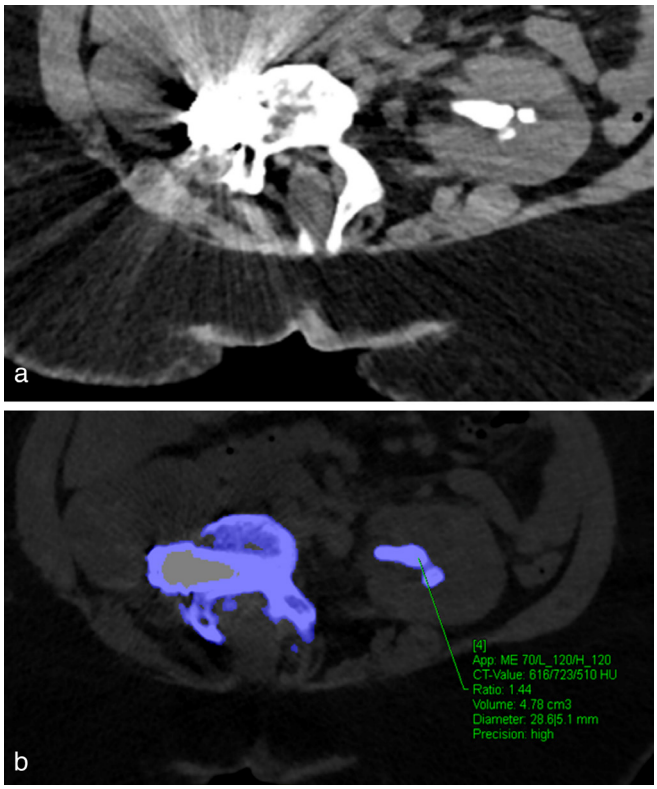

Further radiation dose reduction can be achieved through "spectral shaping," a technique that is not novel to PCD-CT.[68–72] Spectral shaping is most effectively utilized in imaging bone and lung parenchyma, where a tin filter is used to filter out the low energy photons that are mostly absorbed by biologic tissues, but do not contribute appreciably to image signal.[14,68,73] This technique has been shown in the literature to produce non-contrast chest CT images of diagnostic image quality in pediatric patients, including inspiratory and expiratory phases, down to a mean effective dose of 0.12 ± 0.04 mSv, with a CTDIvol of 0.07 ± 0.03 mGy per scan.[29,30] Figure 6 shows an ultra-low dose CT in a patient with cystic fibrosis (CTDIvol of 0.05 mGy); it also shows a radiation dose reduction of about 50% in same-day, EID *vs* PCD high-resolution chest CTs in another pediatric patient. Additional applications for low-dose imaging are relevant wherever reduced dose imaging is a high priority, such as in patients that require serial CT imaging or have increased sensitivity to radiation. Low-dose PCD-CT imaging with a tin filter has also shown radiation dose reductions compared to EID-CT of up to 85% in the temporal bone CT,[14,74] 67% in sinus CT,[14] 50% in imaging femoral acetabular impingement,[75] and 66% in high-resolution lung imaging in adults.[76]

IMPROVED IODINE SIGNAL

Unlike EID-CT, where the signal recorded is the summation of all photon energies, individual incident photons and their energy information are recorded in PCD-CT.[10] The photon counting detection mechanism allows for lower energy photons, which carry more iodine signal, to be more optimally weighted in the output signal than in EID-CT,[77] thereby increasing iodine SNRs.[12]

Strategies to increase iodine signal at CT have long incorporated the concept that iodine attenuation increases at lower photon energies, which in EID-CT is typically accomplished using lower tube potentials.[78–82] Phantom studies demonstrated a mean increase in iodine CNR of 11, 23, 31, and 38% at 80, 100, 120, and 140 kV in PCD-CT over EID-CT.[12]

Figure 11. A 16-year-old male with a suspected coronary anomaly. Cardiac multienergy PCD scan reconstructions at (a) 40 keV, (b) 50 keV, (c) 100 keV, (d) color-coded iodine overlay, (e) iodine overlay and (f) VNC. No coronary anomaly was detected but a short segment myocardial bridge (arrow) of the distal left anterior descending artery at the level of the apex was detected as shown in image (g). PCD, photon counting detector; VNC, virtual non-contrast.

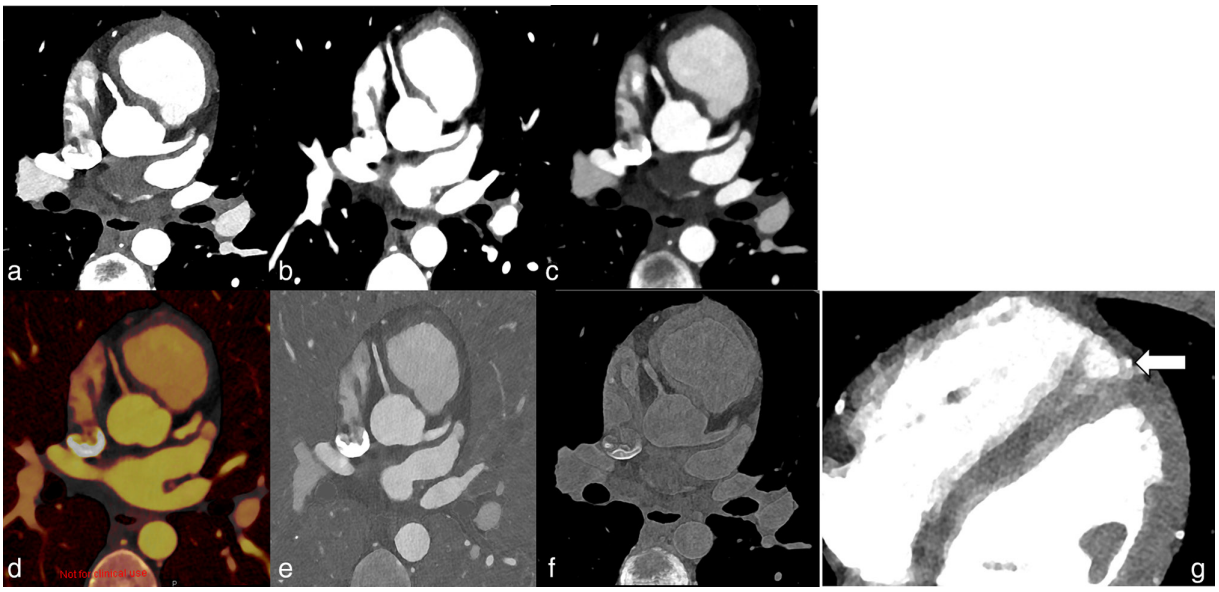

With its energy-resolved information, PCD-CT also allows for the reconstruction of virtual monoenergetic images (VMIs) corresponding to lower photon energies, just as is done in dual-energy CT. Studies have documented up to 75% higher CNR for VMIs below 60 keV obtained at 90kV.[83] Multiple studies in adults have suggested 45–50 keV as the optimal VMI range to assess small vessels, the

Figure 12. A 17-year-old female with a history of neurogenic bladder, scoliosis, and secondary xanthogranulomatous pyelonephritis of the right kidney. Clinical conventional EID CT scan demonstrating the known kidney pathology with streaking artifacts from spinal metal hardware (arrows) (a). Figures (b–e) show different PCD-CT reconstructions; 120 kV PCD-CT image, also showing streak artifacts [arrows] (b), with 130 keV (c), IMAR threshold low (d), and threshold high (e) images demonstrating several alternatives at PCD for minimizing metallic artifact like using high energy VMIs, IMAR images, threshold high images (which are reconstructed using high-energy incident photons). CTDI vol for EID-CT scan 3.11 mGy *vs* 2.49 mGy for PCD-CT. EID, energy integrated detector; IMAR, iterative metal artifact reduction; PCD, photon counting detector; VMI, virtual monoenergetic image.

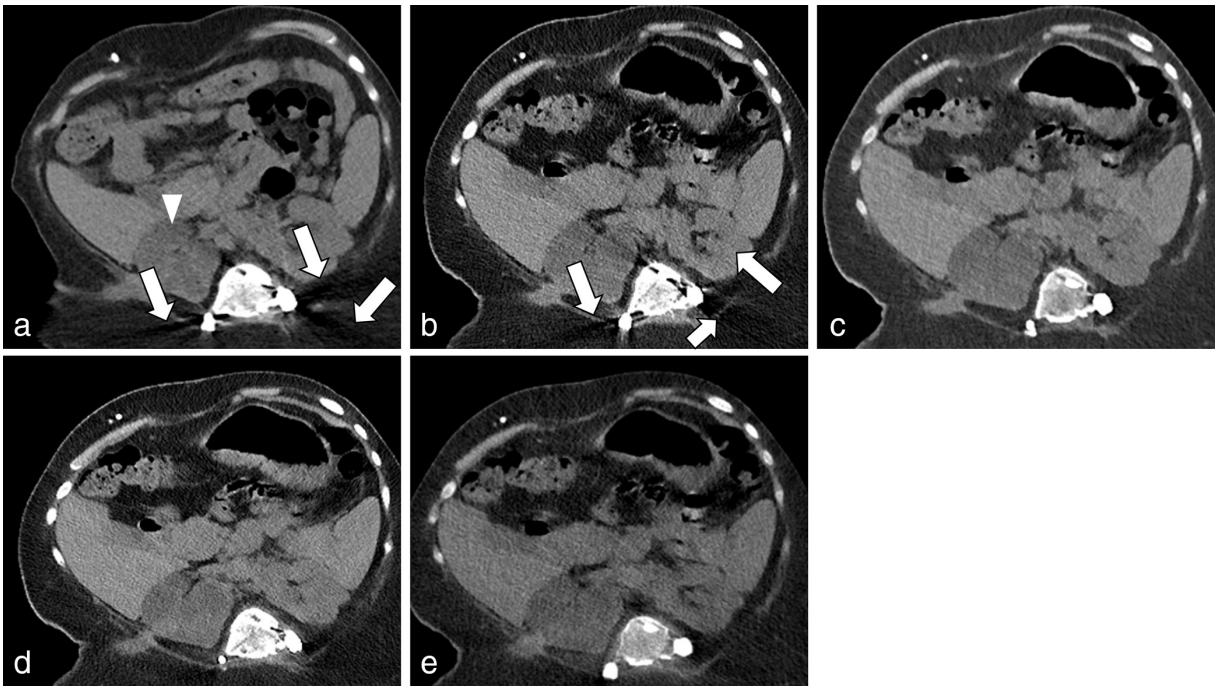

aorta, and the visualization of pulmonary emboli.[84–88] Low keV VMIs also have been demonstrated to increase conspicuity of hypovascularized hepatic metastases through improved iodine CNR.[89] From physics principles, the effect should be even more pronounced in small patients, where noise does not increase as dramatically as VMI energy level is decreased.

Because iodine CNR is improved with PCD-CT compared to EID-CT performed with similar scan parameters, there is better visualization of vessels and the interfaces of enhancing tissues on PCD-CT (Figure 7). Cao et al suggests that increased iodine contrast in PCD-CT also could be used to reduce intravenous contrast doses.[28] A contrast media dose reduction of 25% for PCD-CT angiography of the aorta was shown in adult patients to maintain image quality compared to EID-CT images obtained at equivalent radiation doses.[86] Sawall et al. estimated that a reduction in iodinated contrast volume of up to 13–37% is feasible with the greatest reduction seen in larger patient sizes.[90]

MULTIENERGY IMAGING APPLICATIONS

In addition to VMI, the inherent multienergy information acquired by PCD-CT can be used to perform material-specific imaging, including creating iodine maps, virtual non-contrast images (Figure 8b), virtual non-calcium images (Figure 8c, Figure 9), and kidney stone characterization (Figure 10). These applications are similar to those achieved with dual-energy EID-CT. However, PCD-CT offers the ability to perform these tasks with simultaneous high-pitch, high-temporal resolution scanning (*i.e.* in the "Flash" mode), or ultra-high spatial resolution imaging ("UHR" mode), which has not been possible previously.

The combination of inherent spectral capability and high spatial resolution allows for material decomposition of smaller structures with less artifact. PCD-CT has been shown to increase the accuracy of smaller renal stone characterization relative to EID-CT in adults.[91] In addition, the inherent spectral capability of PCD-CT allows for the combination of novel material-specific imaging algorithms and contrast agents, opening up the possibility of visualizing new features of tumor and disease composition.[92–94]

These multienergy capabilities also can be combined with high-pitch (pitch = 3.2) cardiac (66 ms temporal resolution) scanning to simultaneously reduce motion artifact and radiation dose.[7,95,96] One application is to improve the visualization of cardiac anomalies in pediatric patients (Figure 11).

Finally, PCD-CT provides multiple pathways to reducing metallic artifacts (Figure 12), including the use of high energy VMI images, tin filtration, and iterative metal artifact reduction (using either all the incident photons, or only those above a preset energy threshold).[27] Clinical applications include reducing streak artifact for orthopedic hardware, but similar techniques can help eliminate streak artifact from the shoulders or contrast injections.

CONCLUSION

PCD-CT is suited to address many challenges in pediatric imaging. Its superior spatial resolution benefits pediatric patients with their small anatomic structures. The increased dose efficiency is also desirable, with dramatic dose reduction possible for non-contrast imaging with the use of tin filtration, potentially allowing ultra-low-dose CT that replaces plain film radiography for some diagnostic tasks. Improved iodine contrast and VMI may improve detection of subtle abnormalities in oncology, with high pitch imaging negating the need for sedation in some pediatric CT imaging. Further work is needed by the pediatric radiology community to take full advantage of the benefits of PCD-CT for our patients.

ACKNOWLEDGMENTS

The authors wish to thank Kevin Kimlinger for his assistance with manuscript preparation, and study co-ordinators Bolyn Andrist, Ryan Jacobson, and Yong Suk Lee for their contributions to the research team.

COMPETING INTERESTS

The photon counting detector CT scanner used in this work was provided to Mayo Clinic by Siemens Healthineers as part of a sponsored research agreement. Cynthia H. McCollough and Joel G. Fletcher are the recipients of a research grant to institution from Siemens Healthineers. The other authors have no relevant conflicts of interest to disclose.

REFERENCES

1. Bette SJ, Braun FM, Haerting M, Decker JA, Luitjens JH, Scheurig-Muenkler C, et al. Visualization of bone details in a novel photon-counting dual-source CT scanner-comparison with energy-integrating CT. *Eur Radiol* 2022; **32**: 2930–36. https://doi.org/10.1007/s00330-021-08441-4
2. Kämmerling N, Sandstedt M, Farnebo S, Persson A, Tesselaar E. Assessment of image quality in photon-counting detector computed tomography of the wrist - an ex vivo study. *Eur J Radiol* 2022; **154**: 110442. https://doi.org/10.1016/j.ejrad.2022.110442
3. Grunz J-P, Huflage H, Heidenreich JF, Ergün S, Petersilka M, Allmendinger T, et al. Image quality assessment for clinical cadmium Telluride-based photon-counting computed tomography detector in Cadaveric wrist imaging. *Invest Radiol* 2021; **56**: 785–90. https://doi.org/10.1097/RLI.0000000000000789
4. Siegel MJ, Bugenhagen SM, Sanchez A, Kim S, Abadia A, Ramirez-Giraldo JC. Comparison of radiation dose and image quality of pediatric high-resolution chest CT between photon-counting detector CT and energy-integrated detector CT: A matched study. *AJR Am J Roentgenol* 2023; **221**: 363–71. https://doi.org/10.2214/AJR.23.29077
5. Wrazidlo R, Walder L, Estler A, Gutjahr R, Schmidt B, Faby S, et al. Radiation dose reduction in contrast-enhanced abdominal CT: comparison of photon-counting detector CT with 2ND generation dual-source dual-

energy CT in an oncologic cohort. *Acad Radiol* 2023; **30**: 855–62. https://doi.org/10.1016/j.acra.2022.05.021
6. Zhou W, Lane JI, Carlson ML, Bruesewitz MR, Witte RJ, Koeller KK, et al. Comparison of a photon-counting-detector CT with an energy-integrating-detector CT for temporal bone imaging: A Cadaveric study. *AJNR Am J Neuroradiol* 2018; **39**: 1733–38. https://doi.org/10.3174/ajnr.A5768
7. Rajendran K, Petersilka M, Henning A, Shanblatt ER, Schmidt B, Flohr TG, et al. First clinical photon-counting detector CT system: technical evaluation. *Radiology* 2022; **303**: 130–38. https://doi.org/10.1148/radiol.212579
8. Leng S, Rajendran K, Gong H, Zhou W, Halaweish AF, Henning A, et al. 150-mum spatial resolution using photon-counting detector computed tomography technology: technical performance and first patient images. *Invest Radiol* 2018; **53**: 655–62. https://doi.org/10.1097/RLI.0000000000000488
9. Flohr T, Petersilka M, Henning A, Ulzheimer S, Ferda J, Schmidt B. Photon-counting CT review. *Phys Med* 2020; **79**: 126–36. https://doi.org/10.1016/j.ejmp.2020.10.030
10. Willemink MJ, Persson M, Pourmorteza A, Pelc NJ, Fleischmann D. Photon-counting CT: technical principles and clinical prospects. *Radiology* 2018; **289**: 293–312. https://doi.org/10.1148/radiol.2018172656
11. Leng S, Bruesewitz M, Tao S, Rajendran K, Halaweish AF, Campeau NG, et al. Photon-counting detector CT: system design and clinical applications of an emerging technology. *Radiographics* 2019; **39**: 729–43. https://doi.org/10.1148/rg.2019180115
12. Gutjahr R, Halaweish AF, Yu Z, Leng S, Yu L, Li Z, et al. Human imaging with photon counting-based computed tomography at clinical dose levels: contrast-to-noise ratio and cadaver studies. *Invest Radiol* 2016; **51**: 421–29. https://doi.org/10.1097/RLI.0000000000000251
13. Emrich T, O'Doherty J, Schoepf UJ, Suranyi P, Aquino G, Kloeckner R, et al. Reduced iodinated contrast media administration in coronary CT angiography on a clinical photon-counting detector CT system: A phantom study using a dynamic circulation model. *Invest Radiol* 2023; **58**: 148–55. https://doi.org/10.1097/RLI.0000000000000911
14. Rajendran K, Voss BA, Zhou W, Tao S, DeLone DR, Lane JI, et al. Dose reduction for sinus and temporal bone imaging using photon-counting detector CT with an additional tin filter. *Invest Radiol* 2020; **55**: 91–100. https://doi.org/10.1097/RLI.0000000000000614
15. Symons R, Pourmorteza A, Sandfort V, Ahlman MA, Cropper T, Mallek M, et al. Feasibility of dose-reduced chest CT with photon-counting detectors: initial results in humans. *Radiology* 2017; **285**: 980–89. https://doi.org/10.1148/radiol.2017162587
16. Rajendran K, Baffour F, Powell G, Glazebrook K, Thorne J, Larson N, et al. Improved visualization of the wrist at lower radiation dose with photon-counting-detector CT. *Skeletal Radiol* 2023; **52**: 23–29. https://doi.org/10.1007/s00256-022-04117-2
17. Rapp JB, Ho-Fung VM, Ramirez KI, White AM, Otero HJ, Biko DM. Dual-source computed tomography protocols for the pediatric chest - scan optimization techniques. *Pediatr Radiol* 2022; **53**: 1248–59. https://doi.org/10.1007/s00247-022-05468-7
18. Gottumukkala RV, Kalra MK, Tabari A, Otrakji A, Gee MS. Advanced CT techniques for decreasing radiation dose, reducing sedation requirements, and optimizing image quality in children. *RadioGraphics* 2019; **39**: 709–26. https://doi.org/10.1148/rg.2019180082
19. Kino A, Zucker EJ, Honkanen A, Kneebone J, Wang J, Chan F, et al. Ultrafast pediatric chest computed tomography: comparison of free-breathing vs. breath-hold imaging with and without anesthesia in young children. *Pediatr Radiol* 2019; **49**: 301–7. https://doi.org/10.1007/s00247-018-4295-5
20. Hagelstein C, Henzler T, Haubenreisser H, Meyer M, Sudarski S, Schoenberg SO, et al. Ultra-high pitch chest computed tomography at 70 kVp tube voltage in an anthropomorphic pediatric phantom and non-sedated pediatric patients: initial experience with 3(Rd) generation dual-source CT. *Zeitschrift Für Medizinische Physik* 2016; **26**: 349–61. https://doi.org/10.1016/j.zemedi.2015.11.002
21. Tivnan P, Winant AJ, Johnston PR, Plut D, Smith K, MacCallum G, et al. Thoracic CTA in infants and young children: image quality of dual-source CT (DSCT) with high-pitch spiral scan mode (TURBO flash spiral mode) with or without general anesthesia with free-breathing technique. *Pediatr Pulmonol* 2021; **56**: 2660–67. https://doi.org/10.1002/ppul.25446
22. Flohr TG, McCollough CH, Bruder H, Petersilka M, Gruber K, Süss C, et al. First performance evaluation of a dual-source CT (DSCT) system. *Eur Radiol* 2006; **16**: 256–68. https://doi.org/10.1007/s00330-005-2919-2
23. Flohr TG, Leng S, Yu L, Aiimendinger T, Bruder H, Petersilka M, et al. Dual-source spiral CT with pitch up to 3.2 and 75 MS temporal resolution: image reconstruction and assessment of image quality. *Med Phys* 2009; **36**: 5641–53. https://doi.org/10.1118/1.3259739
24. Nehra AK, Rajendran K, Baffour FI, Mileto A, Rajiah PS, Horst KK, et al. Seeing more with less: clinical benefits of photon-counting detector CT. *Radiographics* 2023; **43**: e220158. https://doi.org/10.1148/rg.220158
25. Sartoretti T, Wildberger JE, Flohr T, Alkadhi H. Photon-counting detector CT: early clinical experience review. *Br J Radiol* 2023; **96**(1147): 20220544. https://doi.org/10.1259/bjr.20220544
26. Hsieh SS, Leng S, Rajendran K, Tao S, McCollough CH. Photon counting CT: clinical applications and future developments. *IEEE Trans Radiat Plasma Med Sci* 2021; **5**: 441–52. https://doi.org/10.1109/trpms.2020.3020212
27. Esquivel A, Ferrero A, Mileto A, Baffour F, Horst K, Rajiah PS, et al. Photon-counting detector CT: key points Radiologists should know. *Korean J Radiol* 2022; **23**: 854–65. https://doi.org/10.3348/kjr.2022.0377
28. Cao J, Bache S, Schwartz FR, Frush D. Pediatric applications of photon-counting detector CT. *AJR Am J Roentgenol* 2023; **220**: 580–89. https://doi.org/10.2214/AJR.22.28391
29. Horst KK, Hull NC, Thacker PG, Demirel N, Yu L, McDonald JS, et al. Pilot study to determine whether reduced-dose photon-counting detector chest computed tomography can reliably display Brody II score imaging findings for children with cystic fibrosis at radiation doses that approximate Radiographs. *Pediatr Radiol* 2023; **53**: 1049–56. https://doi.org/10.1007/s00247-022-05574-6
30. Tsiflikas I, Thater G, Ayx I, Weiss J, Schaefer J, Stein T, et al. Low dose pediatric chest computed tomography on a photon counting detector system - initial clinical experience. *Pediatr Radiol* 2023; **53**: 1057–62. https://doi.org/10.1007/s00247-022-05584-4
31. Flohr T, Schmidt B. Technical basics and clinical benefits of photon-counting CT. *Invest Radiol* 2023; **58**: 441–50. https://doi.org/10.1097/RLI.0000000000000980
32. McCollough CH, Rajendran K, Leng S, Yu L, Fletcher JG, Stierstorfer K, et al. The technical development of photon-counting detector CT. *Eur Radiol* 2023; **33**: 5321–30. https://doi.org/10.1007/s00330-023-09545-9
33. Yveborg M, Samei E, Hsieh J, Xu C, Fredenberg E, Danielsson M. Photon-counting CT with silicon detectors: feasibility for pediatric imaging. SPIE Medical Imaging; Lake Buena Vista, FL. imaging: SPIE; 26

February 2009. https://doi.org/10.1117/12.813733
34. Taguchi K, Iwanczyk JS. Vision 20/20: single photon counting X-ray detectors in medical imaging. *Med Phys* 2013; **40**(10): 100901. https://doi.org/10.1118/1.4820371
35. Szeles C, Soldner SA, Vydrin S, Graves J, Bale DS. Cdznte semiconductor detectors for Spectroscopic X-ray imaging. *IEEE Trans Nucl Sci* 2008; **55**: 572–82. https://doi.org/10.1109/TNS.2007.914034
36. Si-Mohamed S, Boccalini S, Rodesch P-A, Dessouky R, Lahoud E, Broussaud T, et al. Feasibility of lung imaging with a large field-of-view spectral photon-counting CT system. *Diagn Interv Imaging* 2021; **102**: 305–12. https://doi.org/10.1016/j.diii.2021.01.001
37. Cormode DP, Si-Mohamed S, Bar-Ness D, Sigovan M, Naha PC, Balegamire J, et al. Multicolor spectral photon-counting computed tomography: in vivo dual contrast imaging with a high count rate scanner. *Sci Rep* 2017; **7**(1): 4784. https://doi.org/10.1038/s41598-017-04659-9
38. Si-Mohamed SA, Boccalini S, Lacombe H, Diaw A, Varasteh M, Rodesch P-A, et al. Coronary CT angiography with photon-counting CT: first-in-human results. *Radiology* 2022; **303**: 303–13. https://doi.org/10.1148/radiol.211780
39. da Silva J, Grönberg F, Cederström B, Persson M, Sjölin M, Alagic Z, et al. Resolution characterization of a Silicon-based, photon-counting computed tomography prototype capable of patient scanning. *J Med Imaging (Bellingham)* 2019; **6**(4): 043502. https://doi.org/10.1117/1.JMI.6.4.043502
40. Flohr TG, Stierstorfer K, Süss C, Schmidt B, Primak AN, McCollough CH. Novel Ultrahigh resolution data acquisition and image reconstruction for multi-detector row CT. *Med Phys* 2007; **34**: 1712–23. https://doi.org/10.1118/1.2722872
41. Siegel MJ, Ramirez-Giraldo JC. Dual-energy CT in children: imaging Algorithms and clinical applications. *Radiology* 2019; **291**: 286–97. https://doi.org/10.1148/radiol.2019182289
42. Baffour FI, Rajendran K, Glazebrook KN, Thorne JE, Larson NB, Leng S, et al. Ultra-high-resolution imaging of the shoulder and pelvis using photon-counting-detector CT: a feasibility study in patients. *Eur Radiol* 2022; **32**: 7079–86. https://doi.org/10.1007/s00330-022-08925-x
43. Hernandez AM, Wu P, Mahesh M, Siewerdsen JH, Boone JM. Location and direction dependence in the 3d MTF for a high-resolution CT system. *Med Phys* 2021; **48**: 2760–71. https://doi.org/10.1002/mp.14789
44. Chen H, Danielsson M, Xu C. Size-dependent scanning parameters (kVp and mAs) for photon-counting spectral CT system in pediatric imaging: simulation study. *Phys Med Biol* 2016; **61**: 4105–26. https://doi.org/10.1088/0031-9155/61/11/4105
45. Symons R, Reich DS, Bagheri M, Cork TE, Krauss B, Ulzheimer S, et al. Photon-counting computed tomography for vascular imaging of the head and neck: first in vivo human results. *Invest Radiol* 2018; **53**: 135–42. https://doi.org/10.1097/RLI.0000000000000418
46. Sigovan M, Si-Mohamed S, Bar-Ness D, Mitchell J, Langlois J-B, Coulon P, et al. Feasibility of improving vascular imaging in the presence of metallic Stents using spectral photon counting CT and K-edge imaging. *Sci Rep* 2019; **9**(1): 19850. https://doi.org/10.1038/s41598-019-56427-6
47. Wehrse E, Sawall S, Klein L, Glemser P, Delorme S, Schlemmer H-P, et al. Potential of Ultra-high-resolution photon-counting CT of bone metastases: initial experiences in breast cancer patients. *NPJ Breast Cancer* 2021; **7**: 3. https://doi.org/10.1038/s41523-020-00207-3
48. Baffour FI, Huber NR, Ferrero A, Rajendran K, Glazebrook KN, Larson NB, et al. Photon-counting detector CT with deep learning noise reduction to detect multiple myeloma. *Radiology* 2023; **306**: 220311: 229–36: . https://doi.org/10.1148/radiol.220311
49. Benson JC, Rajendran K, Lane JI, Diehn FE, Weber NM, Thorne JE, et al. A new frontier in temporal bone imaging: photon-counting detector CT demonstrates superior visualization of critical anatomic structures at reduced radiation dose. *AJNR Am J Neuroradiol* 2022; **43**: 579–84. https://doi.org/10.3174/ajnr.A7452
50. Inoue A, Johnson TF, White D, Cox CW, Hartman TE, Thorne JE, et al. Estimating the clinical impact of photon-counting-detector CT in diagnosing usual interstitial pneumonia. *Invest Radiol* 2022; **57**: 734–41. https://doi.org/10.1097/RLI.0000000000000888
51. Bartlett DJ, Koo CW, Bartholmai BJ, Rajendran K, Weaver JM, Halaweish AF, et al. High-resolution chest computed tomography imaging of the lungs: impact of 1024 matrix reconstruction and photon-counting detector computed tomography. *Invest Radiol* 2019; **54**: 129–37. https://doi.org/10.1097/RLI.0000000000000524
52. Zhou W, Montoya J, Gutjahr R, Ferrero A, Halaweish A, Kappler S, et al. Lung Nodule volume Quantification and shape differentiation with an ultra-high resolution technique on a photon counting detector CT system. *Proc SPIE Int Soc Opt Eng* 2017; **10132**: 101323Q. https://doi.org/10.1117/12.2255736
53. Brenner D, Elliston C, Hall E, Berdon W. Estimated risks of radiation-induced fatal cancer from pediatric CT. *AJR Am J Roentgenol* 2001; **176**: 289–96. https://doi.org/10.2214/ajr.176.2.1760289
54. Goske MJ, Applegate KE, Bell C, Boylan J, Bulas D, Butler P, et al. Image gently: providing practical educational tools and advocacy to accelerate radiation protection for children worldwide. *Semin Ultrasound CT MR* 2010; **31**: 57–63. https://doi.org/10.1053/j.sult.2009.09.007
55. Strauss KJ, Goske MJ, Kaste SC, Bulas D, Frush DP, Butler P, et al. Image gently: ten steps you can take to optimize image quality and lower CT dose for pediatric patients. *AJR Am J Roentgenol* 2010; **194**: 868–73. https://doi.org/10.2214/AJR.09.4091
56. Marin JR, Rodean J, Hall M, Alpern ER, Aronson PL, Chaudhari PP, et al. Trends in use of advanced imaging in pediatric emergency departments, 2009-2018. *JAMA Pediatr* 2020; **174**: e202209. https://doi.org/10.1001/jamapediatrics.2020.2209
57. Wang RC, Kornblith AE, Grupp-Phelan J, Smith-Bindman R, Kao LS, Fahimi J. Trends in use of diagnostic imaging for abdominal pain in U.S. *AJR Am J Roentgenol* 2021; **216**: 200–208. https://doi.org/10.2214/AJR.19.22667
58. NCRP. Medical Radiation Exposure of Patients in the United States: NCRP Report no.184. National Council on Radiation Protection and Measurements. 2019.
59. Kanal KM, Butler PF, Chatfield MB, Wells J, Samei E, Simanowith M, et al. U.S. diagnostic reference levels and achievable doses for 10 pediatric CT examinations. *Radiology* 2022; **302**(1): E6. https://doi.org/10.1148/radiol.2021219027
60. Dirrichs T, Tietz E, Rüffer A, Hanten J, Nguyen TD, Dethlefsen E, et al. Photon-counting versus dual-source CT of congenital heart defects in neonates and infants: initial experience. *Radiology* 2023; **307**(5): e223088. https://doi.org/10.1148/radiol.223088
61. Racine D, Mergen V, Viry A, Eberhard M, Becce F, Rotzinger DC, et al. Photon-counting detector CT with quantum Iterative reconstruction: impact on liver lesion detection and radiation dose reduction. *Invest Radiol* 2023; **58**: 245–52. https://doi.org/10.1097/RLI.0000000000000925
62. Baek J, Pineda AR, Pelc NJ. To bin or not to bin? the effect of CT system limiting resolution on noise and Detectability. *Phys*

Med Biol 2013; **58**: 1433–46. https://doi.org/10.1088/0031-9155/58/5/1433
63. Kachelriess M, Kalender WA. Presampling, algorithm factors, and noise: considerations for CT in particular and for medical imaging in general. *Med Phys* 2005; **32**: 1321–34. https://doi.org/10.1118/1.1897083
64. Klein L, Dorn S, Amato C, Heinze S, Uhrig M, Schlemmer H-P, et al. Effects of detector sampling on noise reduction in clinical photon-counting whole-body computed tomography. *Invest Radiol* 2020; **55**: 111–19. https://doi.org/10.1097/RLI.0000000000000616
65. Yu Z, Leng S, Kappler S, Hahn K, Li Z, Halaweish AF, et al. Noise performance of low-dose CT: comparison between an energy integrating detector and a photon counting detector using a whole-body research photon counting CT scanner. *J Med Imaging (Bellingham)* 2016; **3**(4): 043503. https://doi.org/10.1117/1.JMI.3.4.043503
66. Iwanczyk JS, Nygård E, Meirav O, Arenson J, Barber WC, Hartsough NE, et al. Photon counting energy Dispersive detector arrays for X-ray imaging. *IEEE Trans Nucl Sci* 2009; **56**: 535–42. https://doi.org/10.1109/TNS.2009.2013709
67. Duan X, Wang J, Leng S, Schmidt B, Allmendinger T, Grant K, et al. Electronic noise in CT detectors: impact on image noise and artifacts. *AJR Am J Roentgenol* 2013; **201**: W626–32. https://doi.org/10.2214/AJR.12.10234
68. Zhou W, Bartlett DJ, Diehn FE, Glazebrook KN, Kotsenas AL, Carter RE, et al. Reduction of metal artifacts and improvement in dose efficiency using photon-counting detector computed tomography and tin filtration. *Invest Radiol* 2019; **54**: 204–11. https://doi.org/10.1097/RLI.0000000000000535
69. Takahashi EA, Koo CW, White DB, Lindell RM, Sykes A-MG, Levin DL, et al. Prospective pilot evaluation of Radiologists and computer-aided pulmonary Nodule detection on ultra-low-dose CT with tin filtration. *J Thorac Imaging* 2018; **33**: 396–401. https://doi.org/10.1097/RTI.0000000000000348
70. Leyendecker P, Faucher V, Labani A, Noblet V, Lefebvre F, Magotteaux P, et al. Prospective evaluation of Ultra-low-dose contrast-enhanced 100-kV abdominal computed tomography with tin filter: effect on radiation dose reduction and image quality with a third-generation dual-source CT system. *Eur Radiol* 2019; **29**: 2107–16. https://doi.org/10.1007/s00330-018-5750-2
71. Gordic S, Morsbach F, Schmidt B, Allmendinger T, Flohr T, Husarik D, et al. Ultralow-dose chest computed tomography for pulmonary Nodule detection: first performance evaluation of single energy scanning with spectral shaping. *Invest Radiol* 2014; **49**: 465–73. https://doi.org/10.1097/RLI.0000000000000037
72. Vivier S, Deken V, Arous Y, Faivre J-B, Duhamel A, Deschildre A, et al. Pediatric chest computed tomography at 100 kVp with tin filtration: comparison of image quality with 70-kVp imaging at comparable radiation dose. *Pediatr Radiol* 2020; **50**: 188–98. https://doi.org/10.1007/s00247-019-04543-w
73. Zhou W, Malave MN, Maloney JA, White C, Weinman JP, Huo D, et al. Radiation dose reduction using spectral shaping in pediatric non-contrast sinus CT. *Pediatr Radiol* 2023. https://doi.org/10.1007/s00247-023-05699-2
74. Grunz J-P, Heidenreich JF, Lennartz S, Weighardt JP, Bley TA, Ergün S, et al. Spectral shaping via tin Prefiltration in ultra-high-resolution photon-counting and energy-integrating detector CT of the temporal bone. *Invest Radiol* 2022; **57**: 819–25. https://doi.org/10.1097/RLI.0000000000000901
75. Ferrero A, Powell GM, Adaaquah DK, Rajendran K, Thorne JE, Krych AJ, et al. Feasibility of photon-counting CT for Femoroacetabular Impingement syndrome evaluation: lower radiation dose and improved diagnostic confidence. *Skeletal Radiol* 2023; **52**: 1651–59. https://doi.org/10.1007/s00256-023-04325-4
76. Jungblut L, Euler A, von Spiczak J, Sartoretti T, Mergen V, Englmaier V, et al. Potential of photon-counting detector CT for radiation dose reduction for the assessment of interstitial lung disease in patients with systemic sclerosis. *Invest Radiol* 2022; **57**: 773–79. https://doi.org/10.1097/RLI.0000000000000895
77. Schmidt TG. "Optimal "image-based" weighting for energy-resolved CT". *Med Phys* 2009; **36**: 3018–27. https://doi.org/10.1118/1.3148535
78. NIST. X-Ray Mass Attenuation Coefficients NIST Standard Reference Database 126 database on the Internet. 2004. Available from: https://www.nist.gov/pml/x-ray-mass-attenuation-coefficients (accessed 22 Oct 2022)
79. Siegel MJ, Kaza RK, Bolus DN, Boll DT, Rofsky NM, De Cecco CN, et al. White paper of the society of computed body tomography and magnetic resonance on dual-energy CT, part 1: technology and terminology. *J Comput Assist Tomogr* 2016; **40**: 841–45. https://doi.org/10.1097/RCT.0000000000000531
80. Meyer M, Haubenreisser H, Schoepf UJ, Vliegenthart R, Leidecker C, Allmendinger T, et al. Closing in on the K edge: coronary CT angiography at 100, 80, and 70 kV-initial comparison of a second- versus a third-generation dual-source CT system. *Radiology* 2014; **273**: 373–82. https://doi.org/10.1148/radiol.14140244
81. Nagayama Y, Goto M, Sakabe D, Emoto T, Shigematsu S, Oda S, et al. Radiation dose reduction for 80-kVp pediatric CT using deep learning-based reconstruction: A clinical and phantom study. *AJR Am J Roentgenol* 2022; **219**: 315–24. https://doi.org/10.2214/AJR.21.27255
82. Yu L, Bruesewitz MR, Thomas KB, Fletcher JG, Kofler JM, McCollough CH. Optimal tube potential for radiation dose reduction in pediatric CT: principles, clinical Implementations, and pitfalls. *Radiographics* 2011; **31**: 835–48. https://doi.org/10.1148/rg.313105079
83. Booij R, van der Werf NR, Dijkshoorn ML, van der Lugt A, van Straten M. Assessment of iodine contrast-to-noise ratio in virtual Monoenergetic images reconstructed from dual-source energy-integrating CT and photon-counting CT data. *Diagnostics (Basel)* 2022; **12**(6): 1467. https://doi.org/10.3390/diagnostics12061467
84. Dunning CAS, Rajendran K, Inoue A, Rajiah P, Weber N, Fletcher JG, et al. Optimal virtual Monoenergetic photon energy (keV) for photon-counting-detector computed tomography angiography. *J Comput Assist Tomogr* 2023; **47**: 569–75. https://doi.org/10.1097/RCT.0000000000001450
85. Euler A, Higashigaito K, Mergen V, Sartoretti T, Zanini B, Schmidt B, et al. High-pitch photon-counting detector computed tomography angiography of the aorta: Intraindividual comparison to energy-integrating detector computed tomography at equal radiation dose. *Invest Radiol* 2022; **57**: 115–21. https://doi.org/10.1097/RLI.0000000000000816
86. Higashigaito K, Schmid T, Puippe G, Morsbach F, Lachat M, Seifert B, et al. CT angiography of the aorta: prospective evaluation of individualized low-volume contrast media protocols. *Radiology* 2016; **280**: 960–68. https://doi.org/10.1148/radiol.2016151982
87. Higashigaito K, Euler A, Eberhard M, Flohr TG, Schmidt B, Alkadhi H. Contrast-enhanced abdominal CT with clinical photon-counting detector CT: assessment of image quality and comparison with energy-integrating detector CT. *Acad Radiol* 2022; **29**: 689–97. https://doi.org/10.1016/j.acra.2021.06.018

88. Yalynska T, Polacin M, Frauenfelder T, Martini K. Impact of photon counting detector CT derived virtual Monoenergetic images on the diagnosis of pulmonary embolism. *Diagnostics (Basel)* 2022; **12**(11): 2715. https://doi.org/10.3390/diagnostics12112715
89. Bette S, Decker JA, Braun FM, Becker J, Haerting M, Haeckel T, et al. n.d.).(Optimal Conspicuity of liver metastases in virtual Monochromatic imaging Reconstructions on a novel photon-counting detector CT-effect of keV settings and BMI. *Diagnostics*; **12**: 1231. https://doi.org/10.3390/diagnostics12051231
90. Sawall S, Klein L, Amato C, Wehrse E, Dorn S, Maier J, et al. Iodine contrast-to-noise ratio improvement at unit dose and contrast media volume reduction in whole-body photon-counting CT. *Eur J Radiol* 2020; **126**: 108909. https://doi.org/10.1016/j.ejrad.2020.108909
91. Marcus RP, Fletcher JG, Ferrero A, Leng S, Halaweish AF, Gutjahr R, et al. Detection and characterization of renal stones by using photon-counting-based CT. *Radiology* 2018; **289**: 436–42. https://doi.org/10.1148/radiol.2018180126
92. Mannil M, Ramachandran J, Vittoria de Martini I, Wegener S, Schmidt B, Flohr T, et al. Modified dual-energy algorithm for calcified plaque removal: evaluation in carotid computed tomography angiography and comparison with Digital subtraction angiography. *Invest Radiol* 2017; **52**: 680–85. https://doi.org/10.1097/RLI.0000000000000391
93. Zhou Z, Ren L, Rajendran K, Diehn FE, Fletcher JG, McCollough CH, et al. Simultaneous dual-contrast imaging using energy-integrating detector multi-energy CT: an in vivo feasibility study. *Med Phys* 2022; **49**: 1458–67. https://doi.org/10.1002/mp.15448
94. Ren L, Huber N, Rajendran K, Fletcher JG, McCollough CH, Yu L. Dual-contrast Biphasic liver imaging with iodine and Gadolinium using photon-counting detector computed tomography: an exploratory animal study. *Invest Radiol* 2022; **57**: 122–29. https://doi.org/10.1097/RLI.0000000000000815
95. Koons E, VanMeter P, Rajendran K, Yu L, McCollough C, Leng S. Improved Quantification of coronary artery Luminal stenosis in the presence of heavy Calcifications using photon-counting detector CT. *Proc SPIE Int Soc Opt Eng* 2022; **12031**: 120311A. https://doi.org/10.1117/12.2613019
96. Hausleiter J, Bischoff B, Hein F, Meyer T, Hadamitzky M, Thierfelder C, et al. Feasibility of dual-source cardiac CT angiography with high-pitch scan protocols. *J Cardiovasc Comput Tomogr* 2009; **3**: 236–42. https://doi.org/10.1016/j.jcct.2009.05.012